International Journal of Engineering Inventions
e-ISSN: 2278-7461, p-ISSN: 2319-6491
Volume 15, Issue 4 [April 2026] PP: 82-89

Thermal Performance Evaluation of a Hybrid Liquid–PCM Cooling Structure for Electric Vehicle Batteries

Nguyen Trong Hieu[1], Nguyen Thuy Hang[2], Luu Kieu Oanh[3]
Thai Nguyen University of Technology

Abstract:
Battery Thermal Management Systems (BTMS) for electric vehicles have become increasingly critical in ensuring battery performance and safety. However, conventional cooling methods are typically employed individually, which leads to certain limitations in heat dissipation effectiveness. In this study, a hybrid cooling structure combining a wavy coolant channel and a tubular composite phase change material (PCM) is proposed to enhance thermal management performance.
A three-dimensional heat transfer model is developed to evaluate and compare the cooling performance of two cases: with PCM and without PCM under identical operating conditions. The results indicate that the integration of PCM significantly improves thermal performance, with a reduction in the maximum temperature by 7.493 K and a more uniform temperature distribution among battery cells compared to the case without PCM. This improvement is attributed to the latent heat absorption capability of PCM, which effectively suppresses temperature rise during battery operation.
The findings demonstrate the potential of the hybrid liquid–PCM cooling system in enhancing thermal management efficiency for electric vehicle batteries
Keywords*: Hybrid thermal management, liquid cooling, phase change material, heat generation rate, temperature uniformity.*

Date of Submission: 08-04-2026 Date of acceptance: 21-04-2026

I. Introduction

In recent years, the depletion of conventional energy resources, together with environmental pollution, has become a global challenge. These issues are primarily attributed to greenhouse gas emissions and the widespread use of fossil fuels [1]. Such impacts not only accelerate climate change but also degrade air quality in many countries. In response, the transition toward clean energy sources and the restructuring of energy systems have been strongly promoted worldwide. In this context, electric vehicles (EVs) have emerged as a sustainable transportation solution due to their high energy efficiency, zero tailpipe emissions, and their contribution to improving urban air quality.

The energy system of EVs is primarily based on lithium-ion battery packs, which consist of multiple cells operating simultaneously. Energy is stored and released through reversible electrochemical reactions during charge and discharge processes. The battery is a core component that directly determines the performance, driving range, and safety of EVs. However, during operation, lithium-ion batteries generate a significant amount of heat due to internal resistance losses and electrochemical reactions [2]. When the temperature exceeds allowable limits, battery performance degrades, lifespan is shortened, and more critically, thermal runaway may occur, posing serious safety risks such as fire and explosion [3]. Therefore, maintaining the battery temperature within an optimal range through an effective Battery Thermal Management System (BTMS) is essential for modern EVs.

Currently, common battery cooling methods include air cooling, liquid cooling, and phase change material (PCM)-based cooling. Air cooling offers advantages such as simple structure and low cost; however, its heat transfer capability is limited, making it insufficient under high-load conditions [4]. Liquid cooling provides superior heat transfer performance and more precise temperature control, but it suffers from drawbacks such as complex structure, higher cost, and additional energy consumption for fluid circulation [5]. Meanwhile, PCMs possess high latent heat capacity during phase transition, enabling them to reduce the rate of temperature rise and improve temperature uniformity [6], [7]. However, pure PCM has low thermal conductivity, and its cooling effectiveness diminishes once thermal saturation is reached. As a result, single cooling methods struggle to fully meet the requirements for both efficiency and stability under real operating conditions.

To address these limitations, hybrid cooling systems that combine liquid cooling with PCM have been proposed as a promising solution. In such configurations, PCM acts as a temporary heat absorber, while the

liquid coolant is responsible for transporting heat away from the system. This synergy enhances overall heat dissipation performance, improves temperature uniformity, and reduces the risk of overheating [8].

Bai et al. [9] proposed a BTMS combining PCM with liquid cooling and conducted simulations to investigate the effects of parameters such as cell spacing, cooling plate length, flow rate, and PCM melting temperature. The results indicated that liquid cooling effectively reduces the maximum battery temperature, while PCM significantly improves temperature uniformity within the battery module.

Kong et al. [10] designed and evaluated a hybrid BTMS through both experimental and numerical approaches. The study analyzed the influence of cell spacing, number of cooling tubes, and flow rate on cooling performance. The results showed that the maximum battery temperature was maintained below 50°C, and the temperature difference between cells was less than 5°C, even at a discharge rate of 3C and an ambient temperature of 30°C, demonstrating the superior performance of the hybrid system.

Zhang et al. [11] investigated a BTMS for a module consisting of 106 battery cells, comparing three methods: PCM cooling, liquid cooling, and a hybrid PCM–liquid system. The results revealed that the hybrid configuration achieved the best performance, reducing the maximum temperature and improving temperature uniformity, particularly under high-load conditions (5C discharge rate). This confirms the advantages of combining PCM with liquid cooling over single-method approaches.

Therefore, this study focuses on developing a three-dimensional heat transfer model to evaluate the performance of a hybrid liquid–PCM cooling system by comparing two cases: with and without PCM. The findings contribute to clarifying the role of PCM in enhancing heat dissipation performance and provide a basis for designing efficient BTMS for electric vehicles.

II. Modeling method

2.1 Physical model

Figure 1 illustrates the proposed hybrid thermal management system, in which PCM is integrated with liquid cooling. The model configuration consists of a liquid cooling plate and 22 cylindrical 21700 lithium-ion batteries, each of which is surrounded by a layer of PCM.

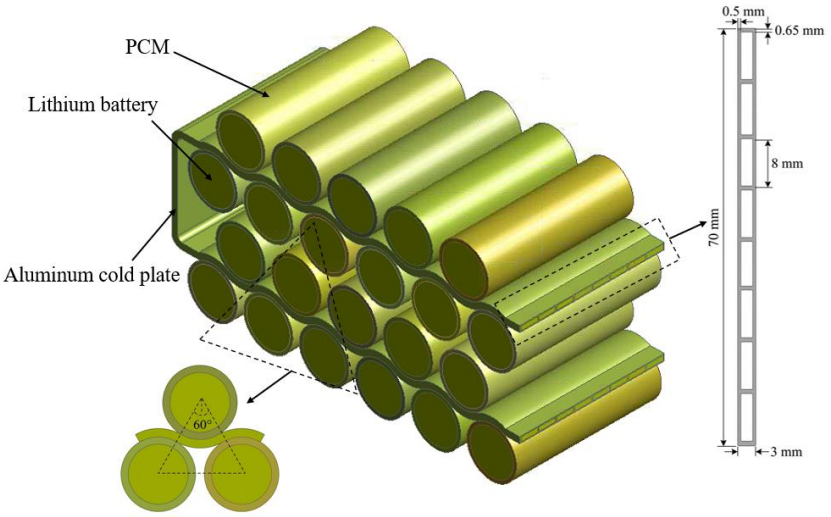

Fig. 1. Physical model of hybrid battery thermal management system.

Each 21700 battery has a diameter of 21 mm and a height of 70 mm. The most critical component of the liquid cooling system is the U-shaped wavy cold plate. From the cross-sectional view, the cold plate consists of eight flow channels, each with a width of 3 mm. The overall height of the plate is 70 mm, which is equal to the height of the batteries. The wall thickness of the cooling plate is 0.5 mm on both sides, while the top and bottom sections have a thickness of 0.65 mm. The inlet section of each channel has a length of 8 mm and a width of 2 mm.

The battery cells are symmetrically arranged on both sides of the wavy cold plate. The contact angle between the encapsulating PCM layer and the liquid cooling plate is 60°. The spacing between adjacent cells depends on the thickness of the PCM layer surrounding each battery. In this system, a water–glycol mixture with a glycol volume fraction of 50% is used as the coolant. Paraffin is selected as the primary phase change material. The thermophysical properties of each component in the BTMS are listed in Table 1.

2.2 Model assumptions and governing equations

To facilitate the numerical analysis, several assumptions are introduced to simplify the mathematical model:

(1) The thermophysical properties of the lithium-ion battery, PCM, cooling plate, and coolant are assumed to be constant and independent of temperature;
(2) The no-slip boundary condition is applied at the solid–liquid interfaces;
(3) The coolant is considered an incompressible Newtonian fluid, and the flow is assumed to be laminar;
(4) Heat transfer includes only conduction and convection, while thermal radiation is neglected.

Table 1
Physical properties of materials [12]

Material	Density ($kg \cdot m^{-3}$)	Specific heat capacity ($J \cdot kg^{-1} \cdot K^{-1}$)	Thermal conductivity ($W \cdot m^{-1} \cdot K^{-1}$)	Dynamic viscosity (Pa·s)	Latent heat ($kJ \cdot kg^{-1}$)	Melting temperature (°C)
Battery	2751	1070	$\lambda_z = 23.34$; $\lambda_r = \lambda_\varphi = 1.15$	–	–	–
Aluminum	2719	871	238	–	–	–
Coolant	1071.11	3300	0.384	0.00339	–	–
PCM	800	2000	0.2	0.005	275	41–44

2.2.1 Liquid cooling domain
The Reynolds number (Re) of the coolant is calculated as follows:

$$Re = \frac{\rho v L}{\mu} \qquad (1)$$

where ρ, v, L and μ denote the density, inlet velocity, hydraulic diameter, and dynamic viscosity of the coolant, respectively. In this study, the maximum coolant velocity is set to 0.1 m/s, corresponding to a Reynolds number lower than 2300; therefore, the flow is considered to be laminar.
The continuity, momentum, and energy equations governing the coolant flow are expressed as follows:

$$\frac{\partial \rho_c}{\partial t} + \nabla \cdot (\rho_c \vec{v}) = 0 \qquad (2)$$

$$\rho_c \left[\frac{\partial \vec{v}}{\partial t} + (\vec{v} \cdot \nabla)\vec{v} \right] = -\nabla p_c + \mu \nabla^2 \vec{v} \qquad (3)$$

$$\rho_c C_{p,c} \frac{\partial T_c}{\partial t} + \rho_c C_{p,c} \nabla (\vec{v} \cdot T_c) = \nabla (\lambda_c \cdot \nabla T_c) \qquad (4)$$

Where $C_{p,c}, v, T_c, \lambda_c$ and μ denote the specific heat capacity, velocity vector, temperature, thermal conductivity, and dynamic viscosity of the coolant, respectively.
2.2.2 Battery domain
The energy equation in lithium battery:

$$\rho_{\text{bat}} C_{p,\text{bat}} \frac{\partial T}{\partial t} = \frac{1}{r}\frac{\partial}{\partial r}\left(\lambda_r r \frac{\partial T}{\partial r} \right) + \frac{1}{r^2}\frac{\partial}{\partial \varphi}\left(\lambda_\varphi \frac{\partial T}{\partial \varphi} \right) + \frac{\partial}{\partial z}\left(\lambda_z \frac{\partial T}{\partial z} \right) + q \qquad (5)$$

Where λ_r, λ_φ và λ_z represent the radial thermal conductivity, circumferential thermal conductivity and axial thermal conductivity of the lithium-ion battery, respectively.*T, t* and *q*are the temperature, time and heat generation rate per unit volume of the battery, respectively. The heat generation rate of a battery is typically determined using either direct or indirect measurement methods. In this study, the heat generation rate of a 21700 lithium-ion battery at a 2.5C discharge rate is adopted from the work of Chen et al. [13]. The heat generation rate is expressed as a seventh-order polynomial function of time and is implemented in the simulation.

The heat generation function of the battery at a 2.5C discharge rate is given as follows:

$$q(t) = -1.4805 \times 10^{24} t^7 + 7.5471 \times 10^{19} t^6 - 1.4943 \times 10^{15} t^5 + 1.4042 \times 10^{12} t^4 - 5.3214 \times 10^{6} t^3 + 3.16 \times 10^{2} t^2 - 67.67 t + 1.7325 \times 10^{5} \qquad (6)$$

2.2.3 Cooling plate

The coolant flow channels are made of aluminum. As the coolant passes through the channels, heat transfer occurs between the fluid and the phase change material (PCM) through the aluminum enclosure, governed by the energy conservation equation:

$$\rho_{\mathrm{Al}} C_{p,\mathrm{Al}} \frac{\partial T_{\mathrm{Al}}}{\partial t} = \lambda_{\mathrm{Al}} \nabla^2 T_{\mathrm{Al}} \text{ (7)}$$

where ρ_{Al} , $C_{p,\mathrm{Al}}$, λ_{Al} and $T_{\max}$ represent the density, specific heat capacity,thermal conductivity, and temperature of aluminum, respectively.

2.2.4 PCM domain

The momentum conservation for composite PCM is given as :

$$\rho_{\mathrm{PCM}} \left(\frac{D\vec{V}}{Dt} \right) = -\nabla P + \nabla \cdot (\mu_{\mathrm{PCM}} \nabla \vec{V}) + \rho_{\mathrm{PCM}} \vec{g} \beta (T - T_{\mathrm{ref}}) + \vec{S} \text{ (8)}$$

where $\vec{V}$, $\vec{g}$, P and β represent the velocity vector, gravity vector, statepressure, and thermal expansion coefficient of the composite PCM. In this study, the value of β is 0.0008 (K^{-1}).

The source term $\vec{S}$ is determined as :

$$\vec{S} = -\frac{(1-f_l)^2}{f_l^3 + 0.001} A_{mush} \vec{V} \quad (9)$$

where f_l is determined as follows:

$$f_l = \begin{cases} 0 & T_{PCM} < T_s \\ \dfrac{T_{PCM} - T_s}{T_l - T_s} & T_s,, T_{PCM},, T_l \\ 1 & T_{PCM} .. T_l \end{cases} \quad (10)$$

where f_l and A_{mush} represent the liquid phase fraction and the mushy constant. The subscripts *s* and *l* represent the solid and liquid-phase of composite PCM, respectively.

The energy equation for composite PCM is given as:

$$\rho_{PCM} \frac{\partial H_{PCM}}{\partial t} = \nabla (\lambda_{PCM} \nabla T_{PCM}) \quad (11)$$

where ρ_{PCM} , H_{PCM} , and λ_{PCM} represent the density, total enthalpy, and thermal conductivity of composite PCM, respectively. The total enthalpy HPCM is defined as :

$$H_{PCM} = h + \Delta H_{PCM} \quad (12)$$

where h is the sensible enthalpy and ΔH_{PCM} is the latent enthalpy and calculated as:

$$h = h_{ref} + \int_{T_{ref}}^{T} C_{p,PCM} dT \quad (13)$$

$$\Delta H_{PCM} = f_l \gamma \quad (14)$$

where h_{ref} represents the reference enthalpy. $C_{p,PCM}$ and γ represent the specific heat capacity and latent heat of composite PCM, respectively.

2.2.5. Boundary conditions

In this study, the inlet temperature is assumed to be constant and equal to the ambient temperature of 30°C.

$$t = 0,\ T(x, y, z) = T_{amb} \quad (15)$$

where T_{amb} denotes the ambient temperature.

During the heat transfer process, the thermal contact resistance between the battery, PCM, and the coolant is neglected. The boundary conditions of the BTMS model are defined as follows:

$$-\lambda_{bat} \frac{\partial T}{\partial n} = -\lambda_{PCM} \frac{\partial T}{\partial n} = -\lambda_{Al} \frac{\partial T}{\partial n} \quad (16)$$

$$-\lambda_{Al} \frac{\partial T}{\partial n} = -\lambda_c \frac{\partial T}{\partial n} + h_c (T_c - T_{Al}) \quad (17)$$

$$-\lambda \frac{\partial T}{\partial n} = h_{amb} (T_{surf} - T_{amb}) \quad (18)$$

where $\frac{\partial T}{\partial n}$ represents the temperature gradient, hc and hamb represent the convective heat transfer coefficients of the coolant and the environment to the surfaces. $h_{amb} = 5W/(m^2.K)$ is adopted in this study. T_{surf} represents the surface temperatures of the cell, composite PCM, and cold plate.

2.3Mesh independence evaluation

Computational Fluid Dynamics (CFD) is a scientific discipline that employs numerical methods combined with computer-based simulations to analyze problems involving the motion of continuous media. Through CFD, it is possible to investigate momentum, heat, and mass transfer processes, as well as physicochemical properties, mechanical characteristics, and the thermodynamic, kinetic, and aerodynamic behavior of the studied medium.

In this study, three-dimensional numerical simulations are performed using ANSYS Fluent 2022 R1. A pressure-based solver is employed for transient analysis, utilizing the SIMPLE algorithm to solve the governing equations and a second-order upwind discretization scheme. In addition, the flow regime is assumed to be laminar, while the energy equation and the solidification/melting model are activated. To ensure convergence, the relaxation factors for momentum, pressure, and liquid fraction are set to 0.3, 0.7, and 0.9, respectively.

For mesh independence validation, the following parameters are used: a PCM thickness of 1.5 mm, a coolant inlet velocity of 0.1 m/s, and a battery discharge rate of 2.5C over a duration of 1000 s. In CFD simulations, both mesh quantity and quality significantly affect the accuracy of the results. Figure 2 illustrates the mesh distribution of the entire BTMS.

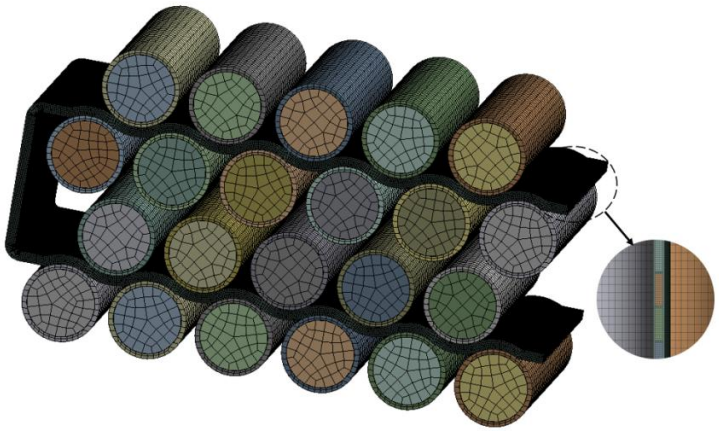

Fig.2. The mesh distribution of the BTMS

In this study, a structured mesh is employed, with a refined meshing strategy to accurately capture the heat transfer process. Additionally, finer mesh elements are applied in the boundary layer regions to better resolve the flow details. Different mesh densities, including 612,269; 1,090,440; 1,793,059; and 2,322,622 elements, are used to examine mesh independence, with the maximum temperature T_{max} selected as the evaluation criterion.

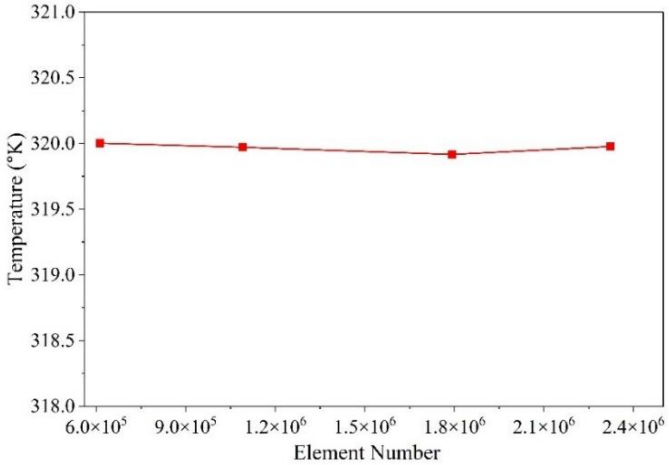

Fig.3. Mesh Independence Evaluation

The results presented in Figure 3 indicate that, as the number of mesh elements increases, the maximum battery temperature remains nearly unchanged, demonstrating that the numerical solution has converged and achieved grid independence. To ensure a balance between computational accuracy and efficiency, the mesh consisting of 1,090,440 elements is selected and used for subsequent analyses.

III. Results and discussion

In this study, the cooling performance of the hybrid thermal management system integrated with PCM is evaluated by comparison with a system using only liquid cooling under identical operating conditions. The boundary conditions are defined as follows: a natural convective heat transfer coefficient of 5 W/(m²·K), a coolant inlet velocity of 0.1 m/s, and an inlet temperature of 30°C. The selected evaluation criterion is the maximum temperature of the entire battery pack at a discharge rate of 2.5C.

Under identical conditions of coolant flow rate, inlet temperature, flow velocity, and discharge rate, the BTMS with and without PCM are numerically simulated and analyzed. Figure 4 illustrates the temperature distribution of the lithium-ion battery pack obtained from the thermal analysis for these two configurations.

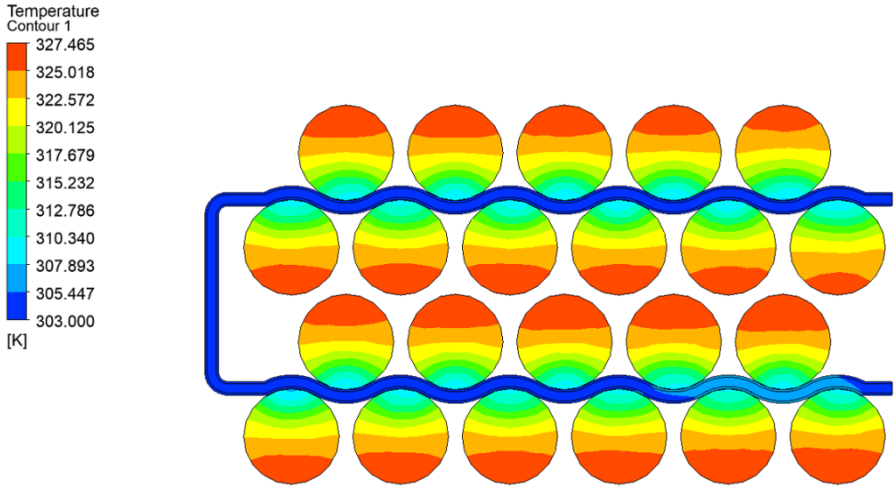

(a) Battery Thermal Management System (BTMS) without PCM

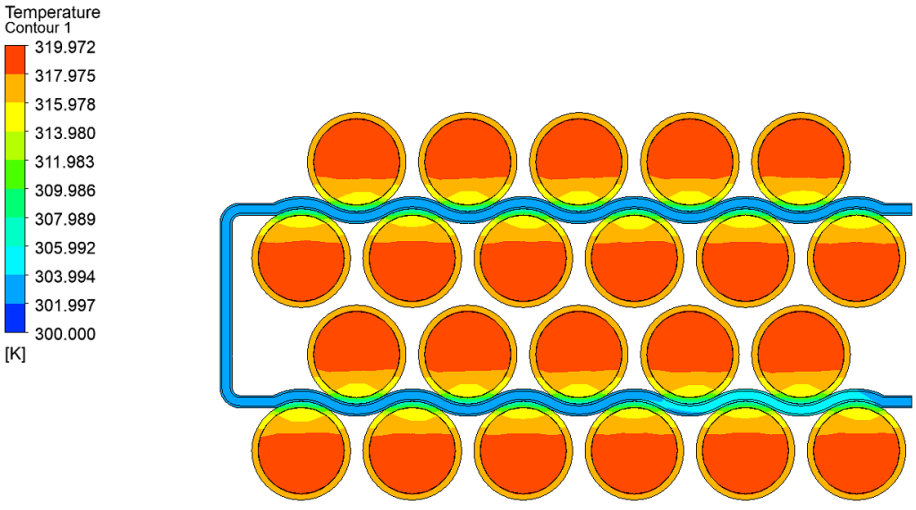

(b) Battery Thermal Management System (BTMS) with PCM

Fig. 4. The temperature distribution cloud diagram of different BTMS

From Figure 4(a), it can be observed that the maximum temperature of the BTMS without PCM reaches 327.465 K, whereas it decreases to 319.972 K for the system with PCM. This reduction of 7.493 K demonstrates that PCM absorbs a significant amount of heat from the battery during the discharge process through latent heat storage, thereby preventing a rapid temperature rise.

In addition to reducing the maximum temperature, it can be seen from Figure 4(b) that the temperature distribution in the system with PCM becomes more uniform compared to the case without PCM. Figure 4(a)

reveals the presence of large temperature gradients both within individual cells and among different cells, as indicated by the pronounced color variation from high- to low-temperature regions. In the system without PCM, the maximum temperature difference (MTD) is 24.465 K, whereas it is reduced to 16.972 K in the system with PCM. Thus, the integration of PCM decreases the MTD by approximately 30.63%, significantly enhancing temperature uniformity within the system.

To further evaluate the effectiveness of PCM, the temperature distribution profiles are analyzed in detail to better elucidate the improvement in thermal uniformity within the battery module.

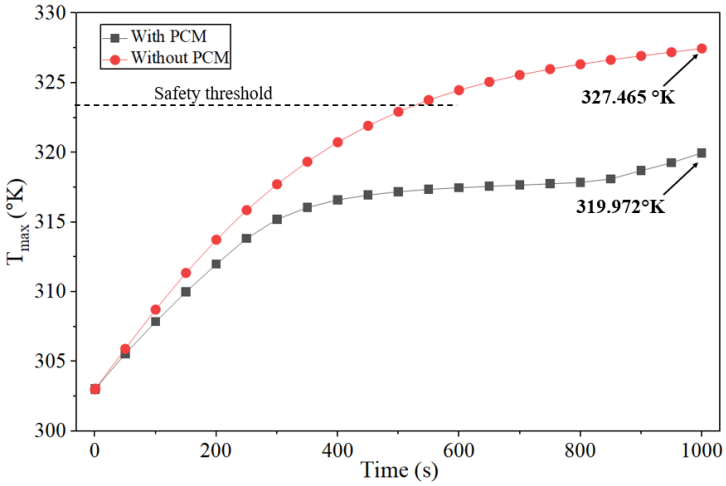

Fig.5. Cooling performance comparison of the battery system with or without PCM.

Figure 5 illustrates the variation of the maximum temperature of the battery module over time for two cases: with and without phase change material (PCM). It can be observed that, during the initial stage ($t < 200$ s), the temperature rise trends of both systems are nearly identical, as the PCM has not yet undergone phase transition and primarily absorbs heat through sensible heat capacity.

However, beyond approximately 200 s, a clear divergence between the two cases becomes evident. For the system without PCM, the temperature increases rapidly and continuously, exceeding the safety threshold of approximately 323 K at around 500–600 s. The maximum temperature reaches about 327.465 K at 1000 s, indicating a significant risk of thermal instability.

In contrast, for the system with PCM, the rate of temperature increase is significantly reduced once the material begins to undergo phase transition. This is attributed to the absorption of a large amount of latent heat during the melting process, which effectively suppresses the temperature rise of the battery. As a result, the maximum temperature only reaches approximately 319.972 K at 1000 s, which is substantially lower than that of the system without PCM and consistently remains below the safety threshold.

Furthermore, the slope of the temperature curve in the range of 300–800 s for the PCM-integrated system remains nearly constant, indicating the effectiveness of passive thermal regulation. In contrast, the system without PCM continues to exhibit a steady temperature increase, reflecting the absence of an efficient thermal storage and regulation mechanism.

From these results, it can be concluded that the integration of PCM into the thermal management system significantly enhances cooling performance, reduces the maximum temperature, and improves the operational safety of lithium-ion battery modules.

IV. Conclusion

This study conducted a numerical simulation to evaluate the performance of a hybrid cooling structure combining liquid cooling and phase change material (PCM) for lithium-ion battery modules. The main findings can be summarized as follows:

- The integration of PCM into the thermal management system significantly reduces the maximum temperature of the battery pack, while the maximum temperature difference (MTD) decreases by approximately 30.63%, indicating improved thermal control capability.
- The PCM-based thermal management system demonstrates clear advantages in enhancing temperature uniformity among battery cells, thereby reducing thermal gradients and improving both the safety and lifespan of the battery.

References

[1]. Intergovernmental Panel on Climate Change (IPCC),Climate Change 2023: Synthesis Report, Geneva, Switzerland, 2023.
[2]. IQAir,World Air Quality Report 2023–2024, IQAir AG, Switzerland, 2024.
[3]. International Energy Agency (IEA),Global EV Outlook 2023, Paris, France, 2023
[4]. X. Feng et al., "Thermal runaway mechanism of lithium-ion battery for electric vehicles: A review," Progress in Energy and Combustion Science, vol. 73, pp. 100–137, 2019.
[5]. M. Ahmadian-Elmi and P. Zhao, "Review of thermal management strategies for cylindrical lithium-ion battery packs," Batteries, vol. 10, no. 2, 2024.
[6]. C. Wu et al., "A review on the liquid cooling thermal management system of lithium-ion batteries," Applied Energy, vol. 375, 2024.
[7]. Z. Ling et al., "Review on thermal management systems using phase change materials for electronic components, Li-ion batteries and photovoltaic modules," Renewable and Sustainable Energy Reviews, vol. 31, pp. 427–438, 2014.
[8]. Shimaa A. Hussien et al., "Enhanced passive thermal management of lithium-ion batteries using phase change materials," Scientific Reports, 2025.
[9]. F. Bai, W. Fang, and Y. Wang, "Thermal performance of a lithium-ion battery pack using a hybrid cooling system combining phase change material and liquid cooling," Journal of Energy Storage, vol. 52, 2022.
[10]. D. Kong, C. Wang, and J. Chen, "Experimental and numerical investigation on a hybrid battery thermal management system combining liquid cooling and phase change material," Applied Thermal Engineering, vol. 201, 2022
[11]. Q. Zhang, Z. Rao, and S. Wang, "Thermal performance of lithium-ion battery module with different cooling strategies: PCM, liquid cooling and hybrid system," Applied Energy, vol. 303, 2021.
[12]. H. Wang, Y. Wang, F. Hu, W. Shi, X. Hu, H. Li, and S. Si, "Heat generation measurement and thermal management with phase change material based on heat flux for high specific energy power battery," Applied Thermal Engineering, vol. 198, 2021, Art. no. 117497.
[13]. H. Chen, G. Wei, L. Xu, and X. Du, "Performance study on a novel hybrid thermal management system for cylindrical lithium-ion battery pack based on liquid cooling and PCM," Energy Conversion and Management, 2025.
[14]. Kumar, Rajeev Ranjan, and Kumar Alok. "Adoption of electric vehicle: A literature review and prospects for sustainability." Journal of Cleaner Production 253 (2020): 119911.
[15]. Sun, Zhiqiang, et al. "Thermal management of the lithium-ion battery by the composite PCM-Fin structures." International Journal of Heat and Mass Transfer 145 (2019): 118739.
[16]. Wang, Jialiang, and Yimin Zhang. "Research on cooling characteristics of power battery fast-charging of refrigerant-based direct cooling system." IOP Conference Series: Earth and Environmental Science. Vol. 696. No. 1. IOP Publishing, 2021.
[17]. Mesbahi, Tedjani, et al. "Coupled electro-thermal modeling of lithium-ion batteries for electric vehicle application." Journal of Energy Storage 35 (2021): 102260.
[18]. Qi Xinrui, et al. "Study of circular, horizontal and vertical elliptical enclosures filled with phase change material in thermal management of lithium-ion batteries in an air-cooled system." Journal of Energy Storage 53 (2022): 105041.
[19]. Sharma, Dinesh Kumar, and Aneesh Prabhakar. "A review on air cooled and air centric hybrid thermal management techniques for Li-ion battery packs in electric vehicles." Journal of Energy Storage 41 (2021): 102885.
[20]. Kim, Byung Ryeon, Thi Nhan Nguyen, and Chan Woo Park. "Cooling performance of thermal management system for lithium-ion batteries using two types of cold plate: Experiment and MATLAB/Simulink-Simscape simulation. International Communications in Heat and Mass Transfer. Số: 145/2023: p:106816.